Water Resources Research

RESEARCH ARTICLE
10.1029/2024WR039606

Multi-Frequency Oscillatory Hydraulic Tomography Improves Heterogeneity Imaging and Resolution and Reduces Uncertainty

Jeremy R. Patterson[1] **and Michael Cardiff**[2]

[1]Department of Earth and Ocean Sciences, University of North Carolina-Wilmington, Wilmington, NC, USA, [2]Department of Geosciences, University of Wisconsin-Madison, Madison, WI, USA

Key Points:

- Different frequencies of periodic testing vary in terms of the volume of aquifer they sample, image, and resolve
- Multi-frequency Oscillatory Hydraulic Tomography (OHT) improves imaging and resolution of aquifer heterogeneity
- Aquifer characterization with OHT requires carefully chosen frequencies to sample aquifers at multiple scales

Supporting Information:

Supporting Information may be found in the online version of this article.

Correspondence to:

J. R. Patterson,
pattersonjr@uncw.edu

Citation:

Patterson, J. R., & Cardiff, M. (2025). Multi-frequency oscillatory hydraulic tomography improves heterogeneity imaging and resolution and reduces uncertainty. *Water Resources Research*, *61*, e2024WR039606. https://doi.org/10.1029/2024WR039606

Received 2 DEC 2024
Accepted 29 APR 2025

Author Contributions:

Conceptualization: Jeremy R. Patterson, Michael Cardiff
Formal analysis: Jeremy R. Patterson
Funding acquisition: Michael Cardiff
Investigation: Jeremy R. Patterson
Methodology: Jeremy R. Patterson, Michael Cardiff
Supervision: Michael Cardiff
Visualization: Jeremy R. Patterson
Writing – original draft: Jeremy R. Patterson, Michael Cardiff
Writing – review & editing: Jeremy R. Patterson, Michael Cardiff

Abstract Understanding subsurface heterogeneity is crucial to predicting groundwater flow pathways, mixing, and other processes in aquifers and other fluid reservoirs. Despite significant effort developing geophysical tools to understand this heterogeneity, geophysical mapping of aquifer flow parameters—transmissivity (T), and storativity (S)—remains challenging due to both uncertainty in petrophysical relationships and resolution/data coverage issues. A more direct approach to mapping heterogeneity over a range of scales is by inducing aquifer flow at various scales and analyzing spatially distributed pressure responses, so-called Hydraulic Tomography (HT). Oscillatory Hydraulic Tomography (OHT) is a recently-developed variant of HT that takes advantage of signal processing routines and fast computational models to reduce data noise impacts and enable high-performance tomography workflows. Laboratory and field studies have demonstrated that OHT tests performed at multiple frequencies appear to improve aquifer imaging results; however, a rigorous analysis of data content, resolution and uncertainty in OHT workflows has not been performed to-date. This work assesses the resolution and uncertainty in single- and multi-frequency OHT testing through numerical experiments and three separate approaches to assessing tomographic resolution: singular value decomposition, geophysical "checkerboard" tests, and stochastic imaging experiments. Contrary to results in some prior published work, all three approaches verify the ability of OHT to image aquifer parameters at resolutions of roughly $\frac{1}{2}$ inter-well spacing distances, and similarly demonstrate the added information provided by multi-frequency data.

Plain Language Summary The natural variability (i.e., heterogeneity) in the underground geologic materials making up aquifers and other fluid reservoirs cannot be "seen" directly, limiting our ability to make accurate predictions about the flow of water and the transport of contaminants throughout the subsurface. Through numerical experiments, this work investigates the ability of a novel technology—Oscillatory Hydraulic Tomography (OHT)—to image this aquifer heterogeneity. We use numerical simulations and imaging experiments to explore the capabilities of OHT, and demonstrate the ability of multi-frequency OHT experiments to improve images of aquifer heterogeneity, in terms of the area which is effectively imaged and the ability to resolve finer-scale features in a reservoir.

1. Introduction

There is an incredible degree of variability in the ability of natural geologic materials to both store and transmit fluids, as well documented in Sanchez-Vila et al. (2006). This large multi-scale variability—and our inability to directly "see" these hydraulic properties—negatively impacts scientists' ability to make accurate predictions about the functioning of the hydrosphere across a range of applications. In the shallow subsurface (≈1 km or less), variability in permeability controls how water enters and exits the subsurface (e.g., the location and intensity of surface water-groundwater interactions) and exerts strong control on solute transport through aquifers. Variation in parameters that impact fluid storage—such as bulk compressibility and porosity—is generally less extreme than variability in permeability, but can similarly affect our understanding of the volumes of water stored underground. Similarly, the large variability in permeability of rocks in the deeper subsurface, controls the fluxes of fluids, solutes, and energy throughout deeper bedrock aquifers, which are common targets for domestic water supplies, alternative energy development (McClure & Horne, 2014; Wu et al., 2021), and subsurface storage (Cuss et al., 2015; Fu et al., 2017; Y. Sun & Tong, 2017; Tsang et al., 2015).

Several decades of advancements in near-surface geophysical tools and methods have improved subsurface imaging capabilities, including improvements to the depth of imaging and the resolution of geologic structures. Still, issues associated with unreliable petrophysical relationships, non-uniqueness in geophysical interpretation, and "difficult" geology (e.g., materials that are electrically highly conductive or resistive) can hamper our ability to rely exclusively on these tools (Binley et al., 2015; Day-Lewis et al., 2017). Said more succinctly, geophysical tools are "not a silver bullet," in seeking to understand geologic structures that impact fluid flow and transport, though due to their speed and low cost they are definitely "worth a shot" (Singha, 2017).

A more direct approach to understanding the geometry of structures that impact fluid flow and transport is to closely monitor the propagation of fluid pressures during hydraulic testing, and to carefully process this data through tomographic imaging—so-called Hydraulic Tomography (HT). Like many geophysical tools, HT flexibly parameterizes variability in aquifer properties, and numerically evaluates how aquifer properties between sources (pumping locations) and receivers (pressure observation points) impact observed data. However, unlike geophysical tools (e.g., electrical resistivity tomography), HT images the aquifer properties that directly impact fluid flow.

As with all tomographic analysis, care is necessary in understanding the quality of data being analyzed and the inherent resolution capabilities of an experimental design—consisting of the network of sources and receivers, the series of tests performed, and the tomographic processing techniques—so that results are not over-interpreted (Bohling & Butler Jr, 2010). Hydraulic tests, in particular, may be over-printed by many other signals that effectively increase the degree of noise in observational data. For example, changes to pumping operations at nearby wells, evapotranspiration signals, earth tides, oceanic tides, or water level changes in nearby surface water bodies all represent hydrologic forcings that can be present in field data and are typically ignored during hydraulic test analysis. The speed of testing during typical geophysical surveys often means that the impact of data noise can be reduced to very low levels by repeatedly performing the same or reciprocal tests (Binley et al., 2015), and by "stacking" or averaging repeated noisy signals. In contrast, typical constant-rate pumping tests are unlikely to be repeated due to the amount of time required per test, which commonly last tens of minutes (e.g., Bohling et al., 2007) to hours (e.g., Tiedeman & Barrash, 2020) depending on the site geology or even lasting multiple days when imaging larger spatial areas (e.g., Illman et al., 2009). Additionally, the typical analyses performed for constant-rate pumping tests require the aquifer to initially be in steady-state conditions; in practice this means that each pumping test must be followed by a significant period of "recovery," increasing the total time required for repeated constant-rate pumping tests. These factors imply that HT analyses of typical constant-rate pumping tests should expect significant noise as a component of observational data. Yet, several HT algorithms and demonstrations of hydraulic tests often assume no or very little noise in the hydraulic signal (e.g., Hou et al., 2023; R. Sun et al., 2013; Vasco et al., 1997; Wang et al., 2021; Yeh & Liu, 2000), likely resulting in an "over-promise" in the imaging and resolution capabilities of HT.

Recent advances in high-speed electronic control of hydraulic field equipment, high-frequency pressure measurements, and high sensing resolution of piezometer data have made more detailed field tests possible (Leven & Barrash, 2022). Oscillatory Hydraulic Tomography (OHT) is one such example, in which flow rates at a pumping well (source) are sinusoidally altered at a user-specified frequency—commonly in the range of 1–0.001 Hz (e.g., Cardiff et al., 2020; Guiltinan & Becker, 2015; Patterson & Cardiff, 2023a; Sayler et al., 2018). The raw pressure signal measured by piezometers (receivers) during OHT testing can now reliably record observational hydraulic head amplitudes of less than 1 mm (Cardiff et al., 2020) at temporal sampling frequencies exceeding 100 Hz, and can be summarized as data representing the amplitude and phase (or Fourier coefficients) of the recorded waves. OHT benefits from the fact that the observed time series with associated measurement error can be filtered in the frequency domain and stripped of all hydraulic signals that are not associated with the user-specified testing frequency using a well developed set of signal-processing tools such as those discussed by Bakhos et al. (2014). Said more mathematically, introduced periodic hydraulic head signals generated during OHT are orthogonal to other spurious signals likely to be present in field data. Similar to "stacking" of a repeated signal, measurement error in OHT data (i.e., Fourier coefficients) is inversely related to the length of the recorded signal (Bakhos et al., 2014; Patterson & Cardiff, 2022a); thereby reducing errors in estimating the amplitude and phase of the received signal as more periodic repetitions are recorded.

Earlier numerical and laboratory studies demonstrated how raw pressure time-series can be processed to extract OHT data—i.e., Fourier coefficients—used as inputs for tomographic imaging, as well as estimates of Fourier

coefficient data errors using linear error propagation theory (Zhou & Cardiff, 2017; Zhou et al., 2016). Similarly, earlier numerical studies demonstrated how steady-periodic or frequency-domain numerical models can provide a fast forward-modeling platform to simulate and analyze OHT data tomographically (e.g., Cardiff, Bakhos, et al., 2013). Applying these analysis and modeling approaches in a field setting, Cardiff et al. (2020) demonstrated that multi-frequency OHT yields more detailed heterogeneity imaging compared to THT, suggesting that the use of multiple frequencies provides additional information content to tomographic imaging problems. That said, OHT imaging results have primarily been presented for individual realizations of aquifer heterogeneity, and a rigorous analysis of this technique with associated reproducible results remains lacking in the literature.

One study, Wang et al. (2021), performed a stochastic analysis of multiple single- and multi-frequency OHT tests, though the data from these tests and the modeling codes are not openly available. Still, according to the results of Wang et al. (2021), "[e]xcitations of different frequencies improve the estimates at some locations and worsen them at others. There is no clear winner or loser for characterizing the detailed parameter variations," suggesting that the information content of different pumping frequencies does not have different sensitivity structures. Similarly, the authors state that "multifrequency …OHT does not increase the resolution of aquifer characterization," suggesting that oscillating tests at different frequencies produce redundant information, which is in direct contradiction with the work of Cardiff, Bakhos, et al. (2013) showing that sensitivity structures vary with the pumping frequency and the work of Patterson and Cardiff (2022b) showing that aquifer imaging can be improved by simultaneously inverting multi-frequency data.

To assess the claims of these prior analyses, we perform an in-depth evaluation of resolution, sensitivity, and overall imaging results using a range of tools commonly applied in geophysical imaging studies. In this paper, we use three separate techniques to assess the ability of single- and multi-frequency OHT experiments to image reservoir heterogeneity: (a) We examine the resolution of OHT using linearized approaches commonly applied in geophysical analysis—such as singular value plots and resolution matrix analyses; (b) We analyze OHT resolution through commonly-applied nonlinear test cases used in geophysical workflows (i.e., checkerboard tests); and finally (c) We apply a nonlinear, stochastic analysis of resolution and uncertainty for a series of stochastically-generated heterogeneity realizations. These test cases, together, provide a rigorous basis for understanding the resolution capabilities of OHT as well as for understanding the trade-off between increased field time and increasing imaging accuracy when multi-frequency testing is considered.

As with any tomographic imaging method, the results of tomography are dependent on numerous modeling choices, including the type of regularization performed, the methods for addressing data error, and tuning parameters that affect how misfit residuals (i.e., Bayesian data likelihood functions) are balanced against regularization, "smoothing," or Bayesian priors. Throughout this work, we employ a consistent approach with, we believe, as few subjective choices as possible. However, in order to allow a more in-depth assessment using other tomographic choices or modeling approaches, we include all computer code necessary to implement and/or modify our analyses.

2. Mathematical Formulation

2.1. Forward Modeling

For the purposes of this work, we focus on OHT applied to imaging two-dimensional (map view) variability in groundwater aquifer properties. Transient, saturated groundwater flow at the field scale (tens of meters) is most commonly simulated assuming constant viscosity, small spatial changes in fluid density, creeping/viscous flow, linear compressible storage, and locally isotropic, heterogeneous permeability. Under these assumptions, the governing equation for fluid flow through porous media is:

$$S(\mathbf{x})\frac{\partial h}{\partial t} = \nabla \cdot (T(\mathbf{x})\nabla h) + q(\mathbf{x},\mathbf{t}) \tag{1}$$

$$\mathbf{x} = [x, y] \tag{2}$$

$$h(\mathbf{x},\mathbf{t}) = \frac{p(\mathbf{x},\mathbf{t})}{\rho_f g} \tag{3}$$

$$T(\mathbf{x}) = \kappa(\mathbf{x})\frac{\rho_f g}{\mu_f} b \tag{4}$$

$$S(\mathbf{x}) = \rho_f g[\beta_r(\mathbf{x}) + \eta(\mathbf{x})\beta_f]\, b \tag{5}$$

Where x, y are spatial coordinates, p is fluid pressure, ρ_f and μ_f are fluid density and viscosity, respectively, g is the gravitational acceleration constant, b is aquifer thickness, $T(\mathbf{x})$ is the heterogeneous aquifer transmissivity (in this case, vertically averaged), $\kappa(\mathbf{x})$ represents the spatially variable intrinsic permeability of the porous media (also vertically averaged), and $S(\mathbf{x})$ represents the heterogeneous storativity (also vertically averaged), which given prior assumptions must be associated with either heterogeneous bulk compressibility $\beta_r(\mathbf{x})$ or heterogeneous porosity $\eta(\mathbf{x})$. Based on poroelastic theory and a fundamental analysis of the physical properties controlling specific storage, Rau et al. (2018) derived bounds on specific storage—across a comprehensive range of aquifer types—of less than 2 orders of magnitude: $2.3 \times 10^{-7}\mathrm{m}^{-1} \leq S_s \leq 1.3 \times 10^{-5}\mathrm{m}^{-1}$. In contrast, permeability—and thus transmissivity—varies by more than 10 orders of magnitude across a similarly comprehensive range of aquifer types (Domenico & Schwartz, 1997; Freeze & Cherry, 1979).

Due to the linearity of Equation 1, the periodic effects of an oscillating source/sink—operating at a known frequency—of fluid inside of a domain Ω with boundaries Γ, can be simulated as:

$$S(\mathbf{x})\frac{\partial h'}{\partial t} = \nabla \cdot (T(\mathbf{x})\nabla h') + q(\mathbf{x}, \mathbf{t}) \quad \forall\, \mathbf{x} \in \Omega, t \geq 0 \tag{6}$$

$$h' = 0 \quad \forall\, t \geq 0, \mathbf{x} \in \Gamma_d \tag{7}$$

$$\nabla h \cdot \mathbf{n} = 0 \quad \forall\, t \geq 0, \mathbf{x} \in \Gamma_n \tag{8}$$

$$q(\mathbf{x}, \mathbf{t}) = \mathrm{Re}[Q(\mathbf{x})\exp(i\omega \mathbf{t})] \quad \forall\, t \geq 0 \tag{9}$$

Where h' is head change associated with the oscillating source/sink only, ω is the angular frequency—$\omega = 2\pi f$ with f is the frequency of the pumping signal—and Re [] represents the real part of the argument. Note that $Q(\mathbf{x})$ may be complex-valued, representing the amplitude and phase of source/sinks within the domain. Instead of simulating these effects transiently, the steady-periodic phasor (Φ) of head changes can be solved using a frequency-domain model:

$$i\omega S(\mathbf{x}) = \nabla \cdot (T(\mathbf{x})\nabla \Phi) + Q(\mathbf{x}) \tag{10}$$

$$\Phi_\omega = 0 \quad \forall\, \mathbf{x} \in \Gamma_d \tag{11}$$

$$\Phi_\omega \cdot \mathbf{n} = 0 \quad \forall\, \mathbf{x} \in \Gamma_n \tag{12}$$

$$h'(x, t) = \mathrm{Re}[\Phi(\mathbf{x})\exp(i\omega \mathbf{t})] \tag{13}$$

Mathematically, solving Equation 10 for $\Phi(\mathbf{x})$ is equivalent to solving for the spatially variable Fourier coefficients of pressure waves created in the aquifer. In other words, Equation 10 allows simulation of the amplitude and phase of head waves throughout the domain using a steady-state modeling framework.

2.2. Linear Analyses

2.2.1. Linearized Sensitivity Calculation

Many tomographic imaging approaches rely on initially analyzing the sensitivity of observations to model parameters. For the case of "linear" imaging, the problem is conceptualized as:

$$\mathbf{y}_{\mathbf{obs}} = \mathbf{y}_{\mathbf{sim}} + \epsilon \tag{14}$$

$$\mathbf{y}_{\mathbf{sim}} = \mathbf{Gs} \tag{15}$$

Where $\mathbf{y}_{\mathbf{obs}}$ $(n \times 1)$ is the measured data, $\mathbf{y}_{\mathbf{sim}}$ $(n \times 1)$ is simulated data, $\mathbf{G}$ $(n \times m)$ is the forward model operator that captures the model physics and experimental design, $\mathbf{s}$ $(m \times 1)$ is model parameters, and ϵ $(n \times 1)$ represents data measurement error (i.e., noise).

For linear problems, $\mathbf{G}$ may be readily designed based on the arrangement of sensors and receivers. For example, in the case of travel-time tomography with straight ray paths, and parameters that are the seismic slowness in a series of grid blocks, each row of $\mathbf{G}$ represents a measurement from a particular source-receiver combination, and elements along the row are computed as the path length within each grid block. The elements of the forward model operator, $\mathbf{G}_{i,j}$ may be thought of as the exact sensitivity of observation number i to parameter number j:

$$\mathbf{G}_{i,j} = \frac{\partial \mathbf{y}_{\mathbf{sim}_i}}{\partial \mathbf{s}_j} \tag{16}$$

Regardless of the chosen imaging or inverse modeling approach, the structure of $\mathbf{G}$ places a fundamental control on the ability to accurately recover model parameters. Therefore analyzing this sensitivity matrix, while not necessarily providing imaging results, is a key step in assessing tomographic problems (e.g., Aster et al., 2018; Bohling, 2009; Paradis et al., 2015, 2024), and provides insight into parameter resolution and identifiability.

The relationship between measured head phasors Φ and aquifer properties T and S—as stated in Equations 10 and 13 above—is nonlinear. Still, the local sensitivity of model observations to model parameters can be evaluated for nonlinear models such as these by calculating the model Jacobian $\mathbf{J}$:

$$\mathbf{J}_{i,j} = \left.\frac{\partial \mathbf{y}_{\mathbf{sim}_i}}{\partial \mathbf{s}_j}\right|_{\mathbf{s}_{\mathbf{curr}}} \tag{17}$$

where $\mathbf{s}_{\mathbf{curr}}$ is a current set of model parameters at which the sensitivity is being evaluated. Commonly for nonlinear problems, a reasonably "non-informative" set of current model parameters, such as homogeneous baseline values for T and S, is used as the linearization point $\mathbf{s}_{\mathbf{curr}}$ (e.g., Bohling, 2009; Paradis et al., 2015; Rawlinson & Spakman, 2016). Analyzing the Jacobian using the same techniques that are applied to linear sensitivity matrices, then, provides a partial perspective on parameter resolution and identifiability in nonlinear problems.

2.2.2. Linearized Resolution Analysis

For any set of tested OHT frequencies, we can represent the resulting Jacobian using the singular value decomposition (SVD) as:

$$\mathbf{J} = \mathbf{U}\mathbf{S}\mathbf{V}^T \tag{18}$$

where $\mathbf{U}$ $(n \times n)$ is composed of orthonormal columns that map to the data space, $\mathbf{V}$ $(m \times m)$ is composed of orthonormal columns that map to the model parameter space, and $\mathbf{S}$ $(n \times m)$ is a diagonal matrix containing non-negative singular values that decrease in magnitude along the diagonal. The magnitude of the singular values gives an indication of the information content each individual singular value contributes to parameter identifiability, with a value of 0 indicating that an individual observation contains no unique information content (Aster et al., 2018; Bohling, 2009; Clemo et al., 2003). The singular values associated with the SVD decomposition of a Jacobian provides an approximated (linearized) perspective on the relative information added by different observations—that is, whether individual observations provide non-redundant information.

SVD also provides a perspective on parameter features that can be identified from data versus those that cannot be identified. While there are many approaches to analyzing this information, a common approach in geophysical applications is resolution matrix analysis. First, we use the SVD to generate a generalized inverse for the Jacobian matrix—the Moore-Penrose pseudoinverse (Aster et al., 2018)—given by:

$$\mathbf{J}^{\dagger} = \mathbf{V}_p \mathbf{S}_p^{-1} \mathbf{U}_p^T \tag{19}$$

in which $\mathbf{S}_p$ is a diagonal matrix containing p non-zero singular values (i.e., a partitioned sub-matrix of $\mathbf{S}$), and $\mathbf{V}_p$, and $\mathbf{U}_p$ represent the partitioned forms of $\mathbf{V}$ and $\mathbf{U}$ with columns $p + 1$ and beyond removed (see Aster et al., 2018). Next, the identifiability of model parameters may be assessed via the parameter resolution matrix ($\mathbf{R}$) as follows:

$$\mathbf{R} = \mathbf{J}^{\dagger}\mathbf{J} = \mathbf{V}_p\mathbf{V}_p^T \tag{20}$$

Direct visualization of the resolution matrix represents one approach to assessing parameter identifiability. The diagonal elements of $\mathbf{R}$ represent the resolution for a single model grid cell and range from zero to one, with a value of one meaning the parameter in that grid cell is perfectly resolved.

When evaluating single- and multi-frequency OHT, consistent with previous studies (Bohling, 2009; Clemo et al., 2003; Paradis et al., 2015), we assume that $\mathbf{J}$ represents the numerically approximated sensitivity matrix with homogeneous model parameters given by the mean parameter values (Table 2). For the purposes of determining maximum possible resolution and parameter identifiability in the presence of noise-free data, a pseudo-inverse using the maximum possible p value (i.e., all non-zero singular values) will be used to provide a linearized analysis in later sections. In practice, the number of singular values used during inverse modeling are chosen that allows sufficient parameter variance and fits the data within expected data measurement error without overfitting, the so-called bias-variance tradeoff (Bohling, 2009; Paradis et al., 2015).

2.3. Non-Linear Inverse Modeling

In nonlinear problems, the ability to resolve model parameters cannot be fully captured by a matrix decomposition, as the Jacobian $\mathbf{J}$ is only a local representation of parameter sensitivity. Rather, nonlinear inverse modeling relies on an algorithmic approach to iteratively estimate parameter values until convergence is obtained. Fully understanding the resolution of parameters is thus dependent on studying the behavior of these algorithms.

For this analysis, we followed the quasi-linear geostatistical approach to solve the inverse problem (Cardiff et al., 2009; Kitanidis, 1995). This inversion method performs forward model runs and full Jacobian updates in an iterative manner to minimize the geostatistical objective function given by:

$$\min_{\mathbf{s},\beta} \frac{1}{2}(\mathbf{y} - g(\mathbf{s}))^T \mathbf{Q}_\mathbf{y}^{-1}(\mathbf{y} - g(\mathbf{s})) + \frac{1}{2}(\mathbf{s} - \mathbf{X}\beta)^T \mathbf{Q}_\mathbf{s}^{-1}(\mathbf{s} - \mathbf{X}\beta) \tag{21}$$

where $\mathbf{y}$ $(n \times 1)$ is observed head phasor coefficients, $\mathbf{s}$ $(m \times 1)$ is model parameters, $g()$ is the numerical forward model described by Equation 10 that takes model parameter inputs and outputs predicted head phasors, $\mathbf{Q}_\mathbf{y}$ $(n \times n)$ is the expected data error covariance matrix, $\mathbf{X}$ $(m \times 2)$ is a matrix of drift function values, β (2×1) represents the scalar mean of each aquifer hydraulic parameter (i.e., T and S), and $\mathbf{Q}_\mathbf{s}$ $(m \times m)$ is the expected parameter covariance matrix, defined by the chosen spatial variogram model.

A non-negativity constraint is imposed by perturbing log-transformed parameters during inversion. We declare convergence at the optimal parameters when one of the following two conditions are met: (a) The maximum relative change in the model parameters between successive iterations is less than 1e−3 or (b) The relative change in the objective function value between successive iterations is less than 1e−3.

When performing inverse modeling, the choice of regularization also influences the results of imaging. To impose the fewest possible assumptions during the modeling experiments described herein, we assumed the prior parameter covariance matrix can be described by a linear variogram model, where the slope (i.e., the parameter variance) of the linear variogram is unknown and treated as the regularization parameter. To determine the slope of the linear variogram during our numerical experiments, our approach effectively applied the "discrepancy principle"—commonly used in geophysical applications—to determine the level of regularization at which data is fit suitably. Based on known sensor measurement error, we applied linearized error propagation to calculate the measurement error in signal phasor coefficients, following Bakhos et al. (2014). Then, during inversion, we determined the minimum variogram slope needed to fit observed data (as signal phasors) within the expected measurement error.

Table 1
Model Geometry and Test Design Parameters for Numerical Experiments

Parameter	Value
Model Geometry	
Domain Size	200 × 200 m
Discretization (Δx, Δy)	2 m
Testing Parameters	
Total fluid volume cycled	0.01 m^3
2 periods	10 and 1,600 s
4 periods	10, 50, 300, and 1,600 s
6 periods	10, 50, 90, 300, 700, and 1,600 s

Due to the ill-posed nature of OHT inverse problems, the best parameter estimates represent just one realization consistent with available data. In fact, there are an infinite number of realizations containing the structural features that all "good" realizations have in common, necessitating a rigorous quantification of the uncertainty in our best parameter estimates. Our geostatistical inverse modeling approach is advantageous, in that we have the ability to directly quantify model parameter uncertainty through the posterior covariance matrix:

$$\mathbf{Q}_{s|y} = \mathbf{Q}_s - \begin{bmatrix} \mathbf{J}\mathbf{Q}_s \\ \mathbf{X}^T \end{bmatrix}^T \begin{bmatrix} \mathbf{J}\mathbf{Q}_s\mathbf{J}^T + \mathbf{Q}_y & \mathbf{J}\mathbf{X} \\ (\mathbf{J}\mathbf{X})^T & 0 \end{bmatrix}^{-1} \begin{bmatrix} \mathbf{J}\mathbf{Q}_s \\ \mathbf{X}^T \end{bmatrix} \tag{22}$$

The first m diagonal elements of the posterior covariance matrix represent the variance of the transmissivity and the remaining diagonal elements represent the variance of the storativity, allowing direct visualization of parameter uncertainty throughout the model domain. Due to the nonlinear forward model and assumption of local linearity at the optimal parameters, the posterior covariance matrix likely represents an underestimate of model uncertainty (Cardiff et al., 2009). Despite this, we believe this approach provides a useful way to explore the impacts of multi-frequency OHT on parameter uncertainty relative to single-frequency OHT.

3. Numerical Experiments

3.1. Model Description

To explore the ability of single and multi-frequency OHT to image and resolve aquifer heterogeneity we developed a numerical model that simulates oscillatory flow tests through a 2-D semi-infinite, confined aquifer of constant unit thickness—with model geometry described in Table 1—using the steady-periodic formulation of the confined groundwater flow equation (Equation 10). We designated the lateral boundaries as constant-head boundaries (Equation 11). The modeling domain contains nine fully penetrating wells in a regular 3 × 3 grid pattern with 20 m spacing between adjacent wells.

Each oscillatory flow test consists of a pumping signal generated at one well, while the model simulates the steady-periodic head phasor (Φ) at all observation locations. We specify pumping frequencies spanning more than two orders-of-magnitude that are consistent with previous field experiments (Cardiff et al., 2020; Guiltinan & Becker, 2015; Patterson & Cardiff, 2023a; Sayler et al., 2018) and are sufficiently spaced, such that they have differing sensitivity structures and add non-redundant information during inverse modeling. For each pumping frequency, we rotate the pumping location across each well to generate all possible source-receiver combinations without repetition (i.e., we do not analyze reciprocal signals), which generates a total of 36 observation signals per frequency component. For each oscillatory flow test, we control the amplitude of the pumping signal by specifying the total fluid volume cycled during one full period (Table 1), which is chosen to generate flow rates that are consistent with previous field experiments (Cardiff et al., 2020; Guiltinan & Becker, 2015; Patterson & Cardiff, 2023a). Using this approach, the amplitude of the pumping signal, and thus the amplitude of the observation signals, decreases as the frequency of the pumping signal decreases, providing a conservative estimate of imaging and resolution capabilities associated with OHT. We utilized OHT3DINV (Cardiff, 2016)—an open-source, MATLAB-based, steady-periodic numerical forward model—for all numerical forward and inverse modeling.

Table 2
Heterogeneous Aquifer Geostatistical Parameters

Parameter	Value	Units
Mean transmissivity $(\log_{10}[T])$	−4	$\log_{10}(m^2/s)$
Transmissivity variance $(\log_{10}[T])$	0.9	$[\log_{10}(m^2/s)]^2$
Mean storativity $(\log_{10}[S])$	−4.9	$\log_{10}(-)$
Storativity variance $(\log_{10}[S])$	0.2	$\log_{10}(-)$
X correlation length (L_x)	20	m
Y correlation length (L_y)	20	m

To more closely approximate head data collected under field conditions, we converted the simulated head phasor to a time series of head measurements (Equation 13) with a testing time of 5 complete periods for each frequency component, balancing the trade-off between minimizing data uncertainty and the total time required for testing (Bakhos et al., 2014; Patterson & Cardiff, 2022a). We then added zero-mean Gaussian noise with 0.5 mm standard deviation to the time-series of head measurements to be consistent with

current fiber-optic pressure transducer measurement error (Leven & Barrash, 2022; Patterson & Cardiff, 2023a). Finally, we extracted the head phasors from the noisy observation signal—which serves as the data during tomographic inverse modeling as described in Section 2.3—and quantified the data measurement error by applying linear error propagation theory to calculate the data error covariance matrix ($\mathbf{Q}_y$), following Bakhos et al. (2014).

To verify numerical model accuracy and ensure that the hydraulic boundaries do not impact the numerical solution within the area of interest (i.e., within the well field), we compared the numerically simulated head phasors in a homogeneous aquifer (Table 2) with modeled head phasors given by the steady-periodic analytical model for periodic flow through a fully confined and homogeneous aquifer as presented by Rasmussen et al. (2003). The numerical head amplitudes differed from the analytical head amplitudes by less than 1 mm across the range of tested oscillation periods (Table 1). Based on current high-precision sensor technology, this level of modeling error cannot be differentiated from data measurement error (Leven & Barrash, 2022; Patterson & Cardiff, 2023a).

3.2. Linear Analysis

As an initial approach, we applied the linear analysis techniques described in Section 2.2 to explore the resolution and identifiability of heterogeneous aquifer flow parameters under cases of single- and multi-frequency OHT. While this analysis relies on linearized approaches (and thus does not capture the full non-linear information present in OHT data), it provides evidence for differing parameter sensitivity structures and independent information from oscillatory flow tests conducted at different frequencies.

We first calculated the Jacobian for an OHT survey assuming mean values of homogeneous aquifer parameters $\mathbf{s}_{\mathbf{curr}}$ (Table 2)—consistent with previous approaches (e.g., Bohling, 2009; Clemo et al., 2003; Paradis et al., 2015, 2024)—across the full range of frequencies being analyzed (Table 1). By selecting subsets of rows from the full Jacobian matrix, we can analyze the resolution properties of limited (i.e., single-frequency) testing relative to more complete (i.e., multi-frequency) testing configurations.

Singular value analysis provides a sense of the non-redundant information content associated with each successive singular value by extracting and visualizing the diagonal elements of the singular value matrix (Equation 18). With singular value analysis, a singular value of 0 indicates a data point with no unique information content and the relative amount of independent information provided by a singular value is positively correlated with the value of the singular value. Normalizing the singular values by the largest singular value allows a direct comparison of information content loss across modeling scenarios by comparing the slopes of each singular value spectra, where steeper slopes represent a rapid loss of unique information content with each successive singular value (Bohling, 2009). All of the singular value spectra (single and multi-frequency OHT) overlie each other at the largest singular values (Figure 1), suggesting that the addition of multiple frequencies during OHT is not providing any unique information content at the largest magnitude singular values. The single-frequency OHT singular value spectra shows the greatest slope of all scenarios, suggesting a rapid loss of information content with successive singular values, that is not observed with the multi-frequency OHT singular value spectra (Figure 1). Comparing the relative singular value magnitude at a common singular value index, further highlights the independent information content provided by multi-frequency OHT. For example, considering a singular value index of 60, single-frequency OHT shows the lowest singular value magnitude, and the singular value magnitude increases with increasing number of frequencies used during OHT (Figure 1). These results support the interpretation that multi-frequency hydraulic data adds non-redundant information content that improves parameter identifiability and aquifer heterogeneity imaging.

The singular value analysis above shows the non-redundant information content available with multi-frequency OHT, suggesting that including multiple frequencies during tomographic inverse modeling could improve parameter resolution. To further examine the imaging potential of OHT, we calculated the parameter resolution matrix (Equation 20), where the first m diagonal elements represent the resolution of the transmissivity at each grid cell in the model domain. The areas with greatest resolution cluster around the wells throughout the model domain (Figure 2). The central well contains the highest flow path density during OHT, and therefore shows the highest resolution, independent of the number of frequencies considered (Figure 2). Though transmissivity is not fully resolved at any point in the point in the aquifer, with single or multi-frequency OHT, these results show a positive correlation between the number of frequencies used during OHT and the resulting parameter resolution,

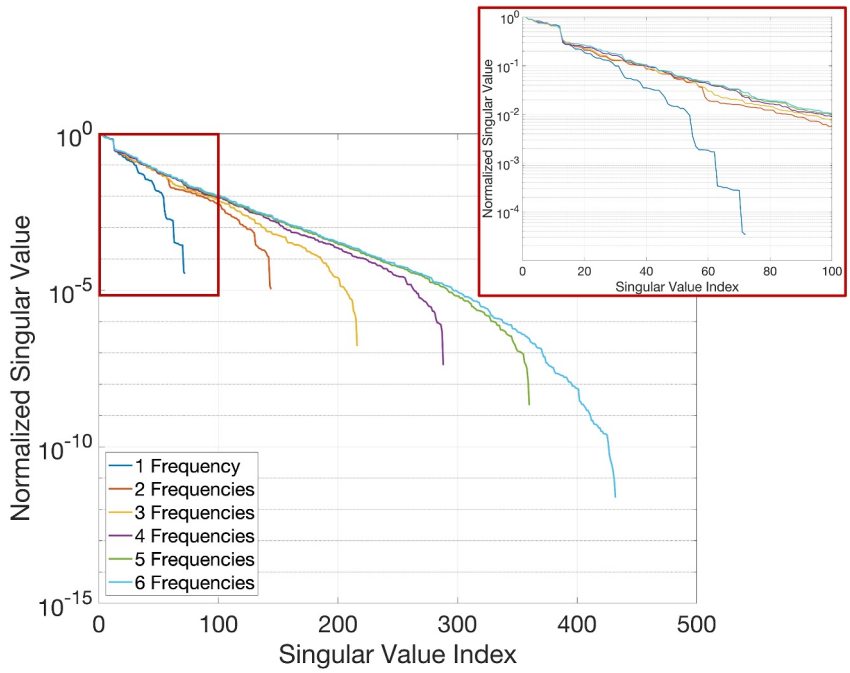

Figure 1. Single and multi-frequency Oscillatory Hydraulic Tomography (OHT) singular value spectra normalized by the largest singular value. For a given number of singular values considered, the magnitude increases with the number of frequencies considered during tomographic analysis, suggesting the additional information content associated with multi-frequency OHT. The inset shows a zoomed in view of the first 100 singular values.

which supports the presence of unique information content, leading to increased parameter identifiability when multiple frequencies are considered during OHT (Figure 2).

Both the singular value spectrum of the Jacobian matrices and the resolution matrix visualization described above are exact representations of imaging capabilities only for the case of linear inverse problems, that is, where data can be represented as linearly resulting from $d = \mathbf{J}s + \epsilon$. Despite this limitation, the results of linear sensitivity

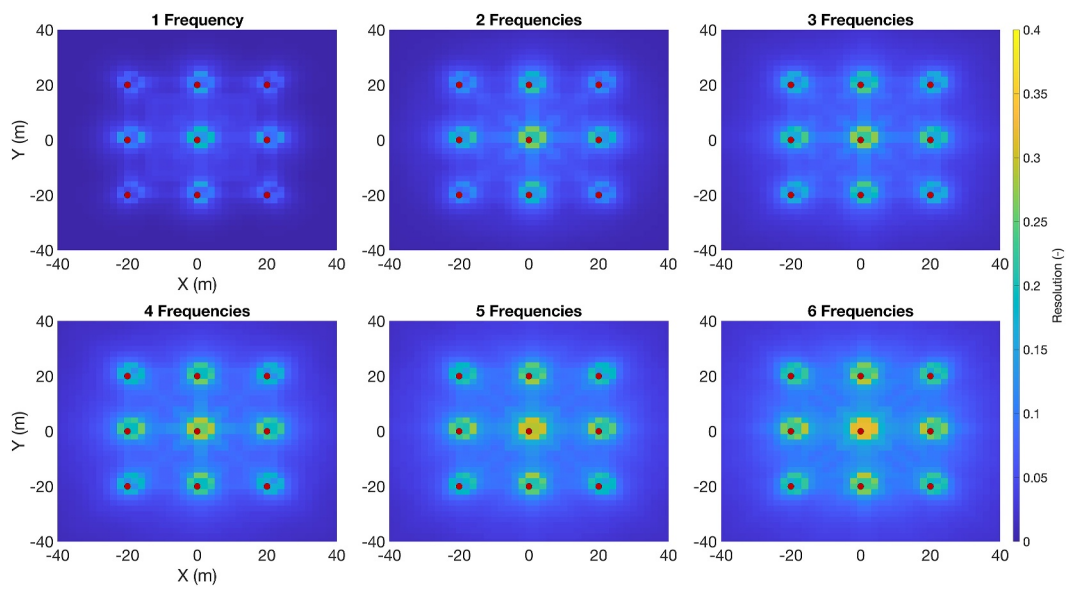

Figure 2. Transmissivity resolution for single- and multi-frequency Oscillatory Hydraulic Tomography, showing increasing resolution with increasing number of frequencies. Red circles represent well locations.

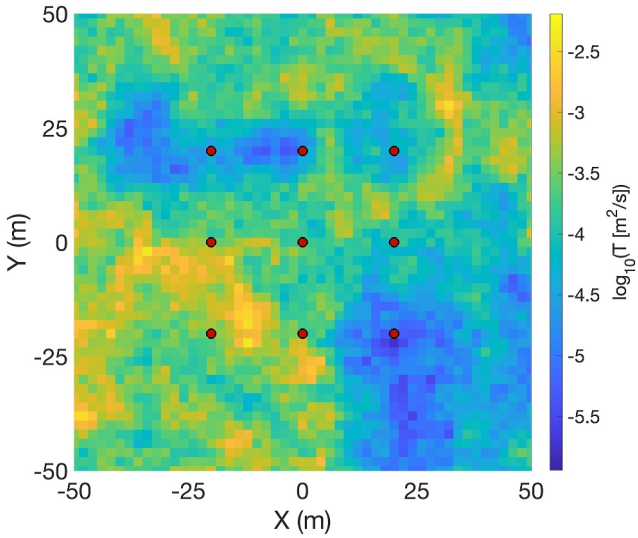

Figure 3. Heterogeneous transmissivity realization used for numerical modeling experiments. Red circles represent well locations.

analysis applied to OHT provides a direct indication that some component of non-redundant information is contained within different testing frequencies, and that some improvement to resolution is provided by multi-frequency OHT data, contrary to the assertion of Wang et al. (2021).

3.3. Imaging Example

While linear analysis approaches provide useful insights that point toward multi-frequency OHT containing additional information, relative to single frequency, that could lead to improved imaging resolution, these approaches are limited by their assumed linear relationship between the physics and model parameters, and their inherent assumption of noise-free signals. To overcome these limitations, we present a non-linear tomographic imaging example designed to further explore the imaging and resolution capabilities associated with multi-frequency OHT. This imaging example inverts for the heterogeneous transmissivity and storativity fields. Because we are interested in comparing trends across single- and multi-frequency OHT imaging results and those trends are consistent across both parameters, we present inverse modeling results for and focus our discussion on transmissivity. Storativity inverse modeling results are available as supplemental information.

For this imaging example, we assumed a heterogeneous transmissivity distribution (Figure 3) that is described by an exponential variogram model with isotropic correlation lengths equivalent to the well spacing (Table 2). We simulated single and multi-frequency OHT (Table 1) to generate steady-periodic head phasors with associated noise and then conducted tomographic inverse modeling as described in Section 2.3. As a quantitative measure to compare inverse modeling performance across tomographic imaging with differing numbers of frequencies, we calculated the Pearson correlation coefficient (i.e., linear correlation) between the true and inverted transmissivity within the area of interest, which includes the total area within the well field as well as the area out to a distance of 20 m beyond the well field in all directions.

Single-frequency OHT inversion performance depends on the input frequency of the pumping signal. High-frequency signals don't propagate beyond the immediate vicinity of the pumping well and thus images the general location of high-transmissivity regions located adjacent to wells throughout the well field, but doesn't capture lower transmissivity regions or larger scale heterogeneous features throughout or beyond the well field (Figure 4a). In contrast, the intermediate- and low-frequency signals propagate throughout the well field and returned very similar tomographic images that capture large scale (i.e., correlation length scale and larger) subsurface structures, while smoothing out smaller scale heterogeneity details throughout the aquifer (Figures 4c and 4e). In all cases the ability to image aquifer heterogeneity using single-frequency OHT is constrained to the well field (Figure 4).

Multi-frequency OHT improves tomographic imaging relative to single-frequency OHT. The use of multiple frequencies during inverse modeling provides greater detail of smaller scale (i.e., less than correlation length scale) aquifer heterogeneities, and also accurately images aquifer heterogeneities beyond the well field (Figure 5). With single-frequency OHT, high transmissivity zones are shown as large, smooth regions throughout the aquifer. Multi-frequency OHT shows separation in these high-transmissivity zones, with four- and six-frequency OHT providing the most detail (Figure 5). Low transmissivity zones in the upper-left and lower-right portions of the well field that were not captured with single-frequency OHT are imaged more accurately in shape, size, location, and orientation (Figure 5). Though there are minor visual detail differences between the tomogram generated with four- and six-frequency OHT, suggesting improvement in heterogeneity imaging, the linear correlation coefficient remains constant across these two scenarios (Figure 5).

The posterior standard deviation in $\log_{10}(T)$ (i.e., parameter uncertainty) provides another quantitative measure of the non-redundant information provided by multi-frequency OHT. Similar to the imaging results described above, transmissivity uncertainty depends on the frequency of the pumping signal with single-frequency OHT. However, the area of lowest parameter uncertainty remains constrained within the well field, regardless of the frequency of the pumping signal (Figure 6). The frequency of the input signal controls the spatial extent of high parameter

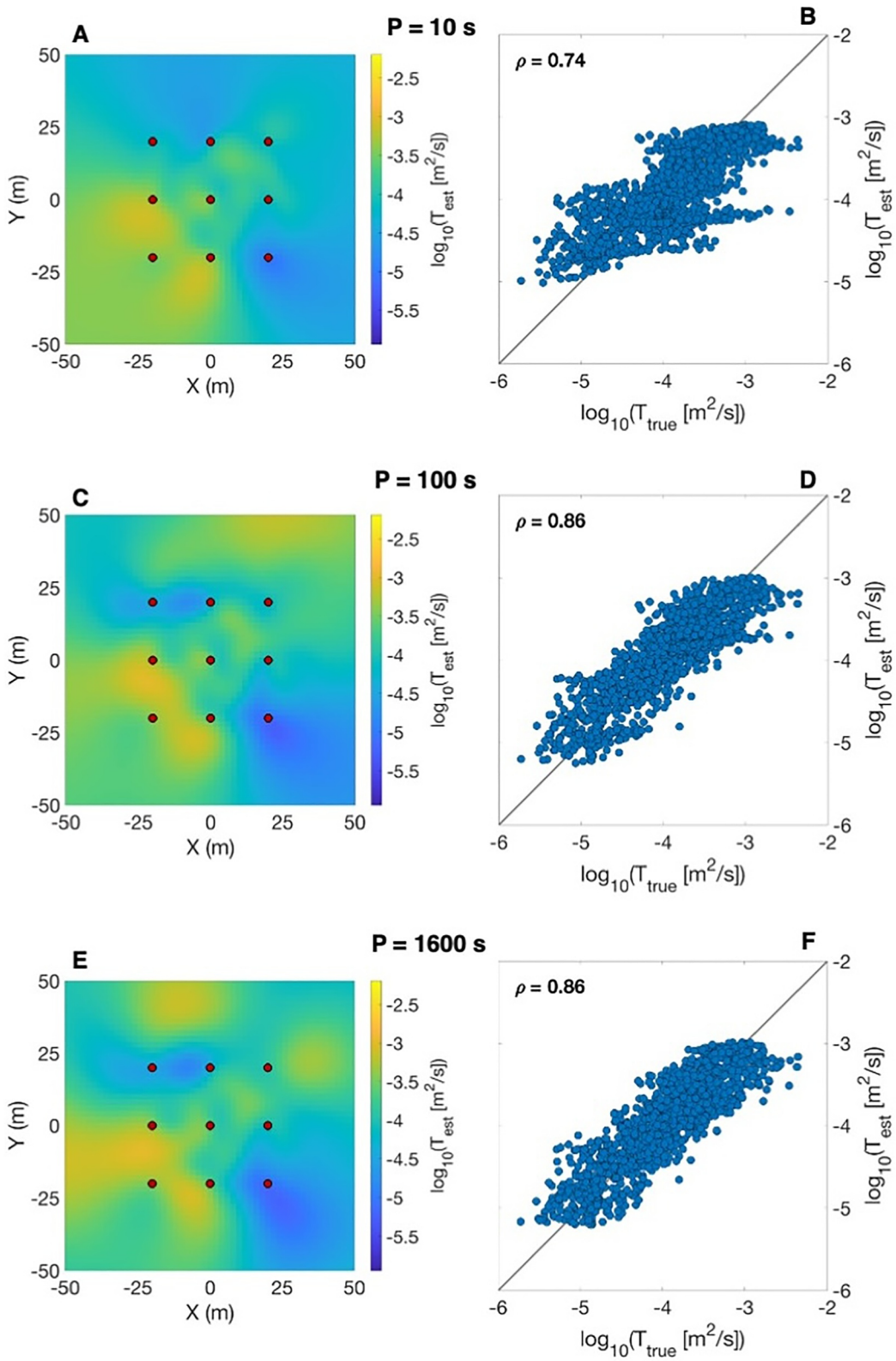

Figure 4. Single-frequency Oscillatory Hydraulic Tomography inverse modeling results. The left column contains the inverted transmissivity tomographic images for (a) high-frequency, (c) intermediate-frequency, and (e) low-frequency pumping signals showing increasing imaging detail as pumping frequency decreases. The right column shows the cross-plot of inverted versus true transmissivity values for (b) high-frequency, (d) intermediate-frequency, and (f) low-frequency pumping signals. Red circles indicate well locations.

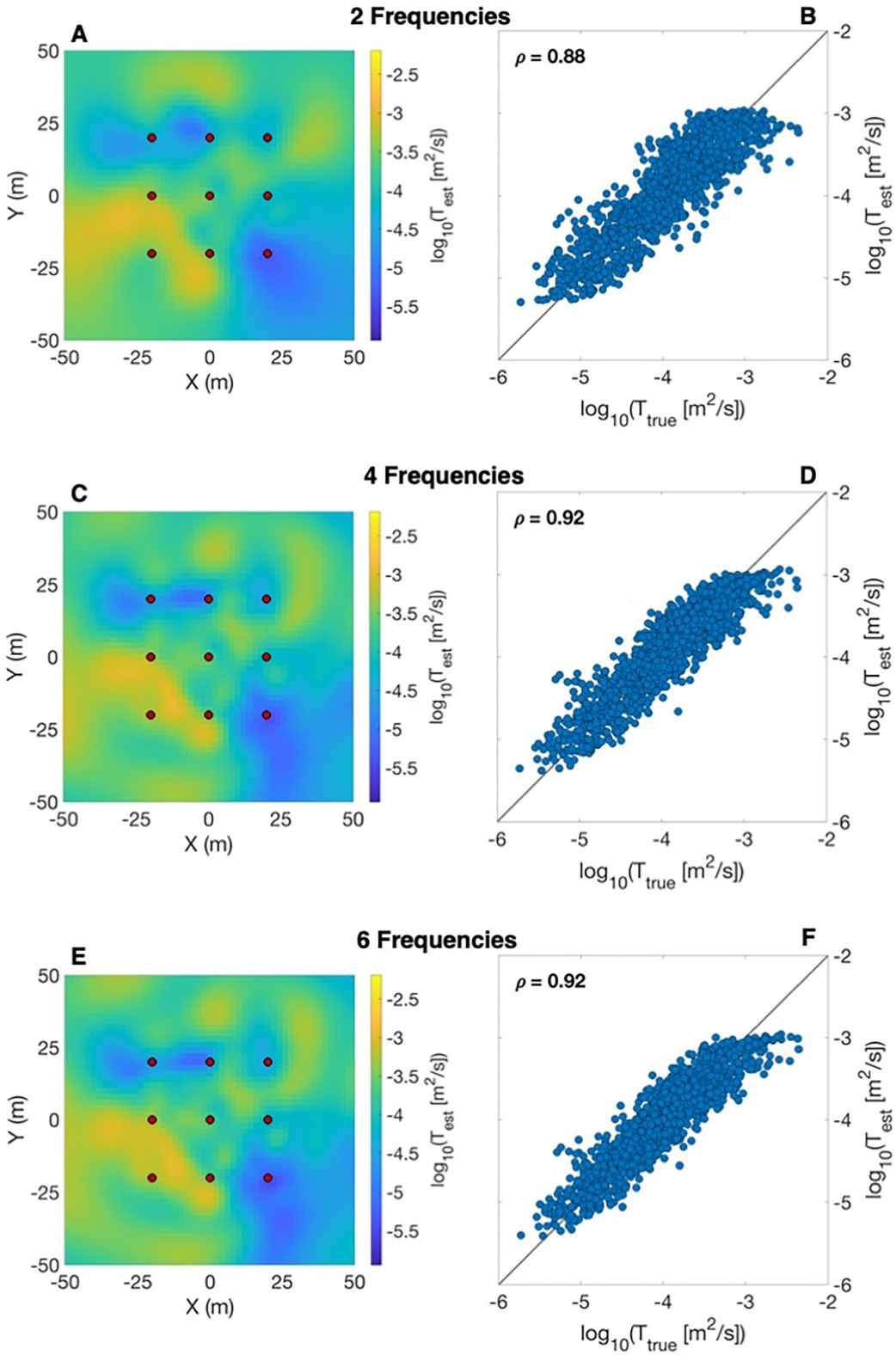

Figure 5. Multi-frequency Oscillatory Hydraulic Tomography (OHT) inverse modeling results. The left column contains the inverted transmissivity tomographic images for multi-frequency OHT with (a) two frequencies, (c) four frequencies, and (e) six frequencies. The right column shows the cross-plot of inverted versus true transmissivity values for multi-frequency OHT with (b) two frequencies, (d) four frequencies, and (f) six frequencies. These results show an improvement in imaging heterogeneity detail and parameter correlation with an increase from two to four frequencies and no improvement when six frequencies are used. Red circles indicate well locations.

uncertainty throughout the domain, with the lowest frequency signals pushing regions of high uncertainty to the edges of the domain (Figure 6). Quantitatively, high-frequency OHT ($P = 10$ s) produces the largest mean parameter uncertainty within the well field of 0.069 $\log_{10}$ (m^2/s), while the intermediate-frequency OHT ($P = 100$ s) produces the lowest mean parameter uncertainty within the well field of 0.063 $\log_{10}$ (m^2/s). With multi-frequency OHT, high uncertainty regions remain at the edges of the model domain, while the low uncertainty region grows beyond the well field and continuously expands as the number of frequencies used during OHT increases (Figure 6. Finally, the mean uncertainty within the well field decreases from 0.060 $\log_{10}(m^2/s)$ with two-frequency OHT to 0.054 a $\log_{10}(m^2/s)$ with six-frequency OHT, a 5% and 15% decrease, respectively, relative to the intermediate-frequency case.

3.4. Stochastic Analysis

The tomographic imaging example shown above provides insight into the imaging capability and resolution associated with multi-frequency OHT for a single realization of aquifer heterogeneity. However, there are an infinite number of heterogeneity realizations consistent with the prescribed geostatistical parameters that will fit the data equally well (Table 2), motivating a stochastic inverse modeling approach to develop an understanding of tomographic imaging performance with single and multi-frequency OHT on average. We generated 100 heterogeneity realizations using the geostatistical parameters given in Table 2 and then conducted inverse modeling for each realization using single- and multi-frequency OHT. As a measure of inversion quality, we calculated the Pearson correlation coefficient and the root mean squared error (RMSE) between the true and inverted transmissivity values for each realization within the area of interest, as defined above.

Multi-frequency OHT improves parameter correlation and reduces modeled parameter error on average and across individual realizations, indicating that each additional frequency component provides non-redundant information content during tomographic imaging. With single-frequency OHT, the correlation coefficient shows large variability that is dominated by relatively low correlation values (Figure 7a). The variability of the correlation coefficient across individual realizations decreases with multi-frequency OHT, with six frequencies showing the lowest variability (Figure 6a). Quantitatively, multi-frequency OHT increases the mean correlation coefficient across all realizations (i.e., the mean value of each column in Figure 7) from 0.85 with single-frequency OHT to 0.87 with six-frequency OHT. Further, multi-frequency OHT shows a clear decrease in modeled parameter RMSE (Figure 7b), with the mean RMSE decreasing from 0.53 $\log_{10}$ (m^2/s) to 0.49 $\log_{10}$ (m^2/s), when comparing single-frequency OHT to multi-frequency OHT conducted with six frequencies.

The spatial distribution of the ensemble mean modeled parameter RMSE shows frequency-dependent behavior similar to the posterior uncertainty estimates above, with the area of the lowest modeled parameter error being confined to the well field, and the largest modeled parameter errors being pushed toward the edge of the domain as the pumping frequency decreases (Figure 8). Similarly, from a quantitative perspective the average modeled parameter error within the well fields decreases from 0.27 $\log_{10}(m^2/s)$ with the high-frequency pumping signal to 0.23 $\log_{10}(m^2/s)$ with the low-frequency pumping signal, a 14% decrease. Again consistent with linearized posterior uncertainty results, the addition of multiple frequencies during OHT sees the area of lowest modeled parameter error growing beyond the well field and further displacing the regions of high modeled parameter error to the edges of the domain (Figure 8). Quantitatively, the mean of the ensemble RMSE within the well field decreases from 0.23 $\log_{10}(m^2/s)$ with single-frequency OHT to 0.20 $\log_{10}(m^2/s)$ with six-frequency OHT, a 13% decrease.

3.5. Checkerboard Testing

The imaging example above demonstrates the additional information content associated with multi-frequency OHT that functions to improve tomographic imaging and reduce parameter uncertainty. In this section, we build on these results to explore the parameter resolution associated with OHT and how the use of multiple frequencies during inverse modeling impacts parameter resolution. Because parameter resolution cannot be represented as a matrix (Equation 20) with highly non-linear problems (Aster et al., 2018), we use a checkerboard test to assess parameter resolution with single- and multi-frequency OHT. The checkerboard test is a commonly used geophysical sensitivity analysis technique where the hydraulic parameters are distributed throughout the model domain in a checkerboard pattern by systematically varying the hydraulic parameters a modest amount above and below the prescribed mean parameter values. For the purposes of this analysis, we

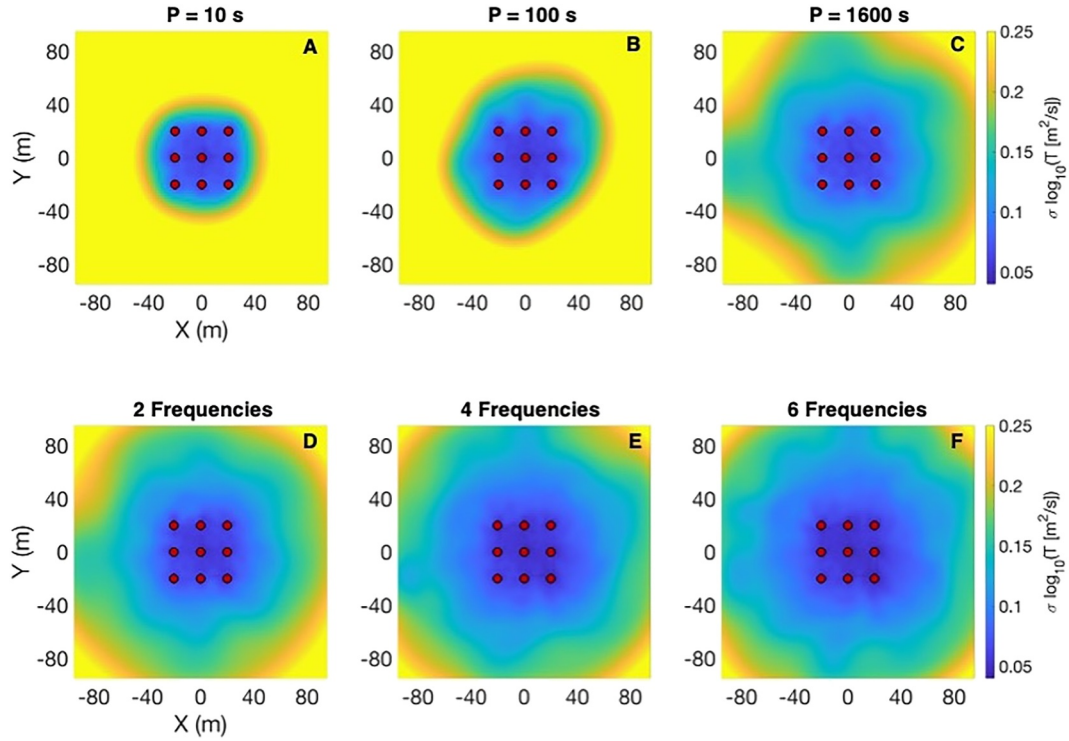

Figure 6. Transmissivity posterior uncertainty estimates. Top row shows uncertainty for single-frequency Oscillatory Hydraulic Tomography (OHT) at (a) high, (b) intermediate, and (c) low frequencies. Bottom row shows uncertainty for multi-frequency OHT using (d) two frequencies, (e) four frequencies, and (f) six frequencies. Red circles represent well locations.

varied $\log_{10}(T)$ by $\pm 5\%$ above and below the mean value and $\log_{10}(S)$ by $\pm 2.5\%$ above and below the mean value (Table 2). The size of the individual checker patterns are typically chosen to match the smallest expected structural features in the area of interest (Hearn & Ni, 1994; Rawlinson & Spakman, 2016; Zelt, 1998). The checkerboard model is used to generate OHT data with associated noise as described in Section 3.1, and then

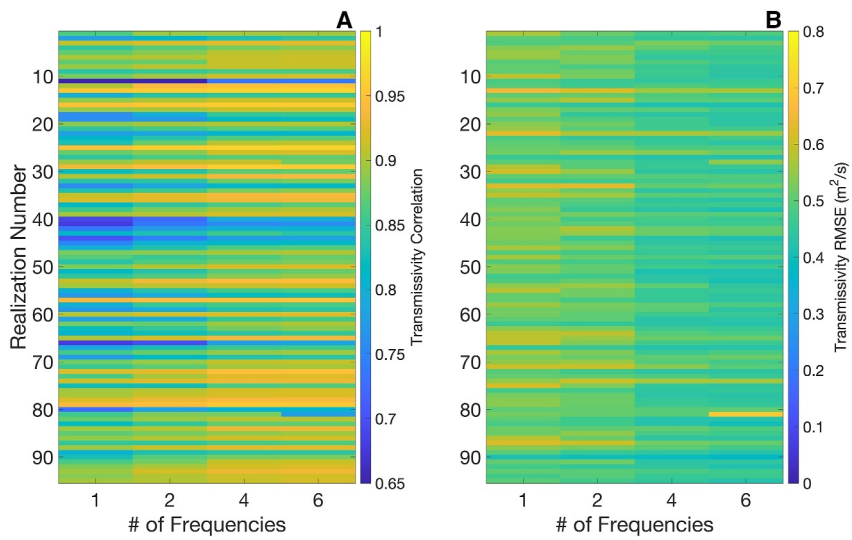

Figure 7. Stochastic inversion quality metrics. (a) Transmissivity correlation for each individual realization showing increased parameter correlation with multi-frequency inversion. (b) Parameter root mean squared error for each realization showing a decrease in parameter error with multi-frequency Oscillatory Hydraulic Tomography. Single frequency realizations are conducted using $P = 1{,}600$ s.

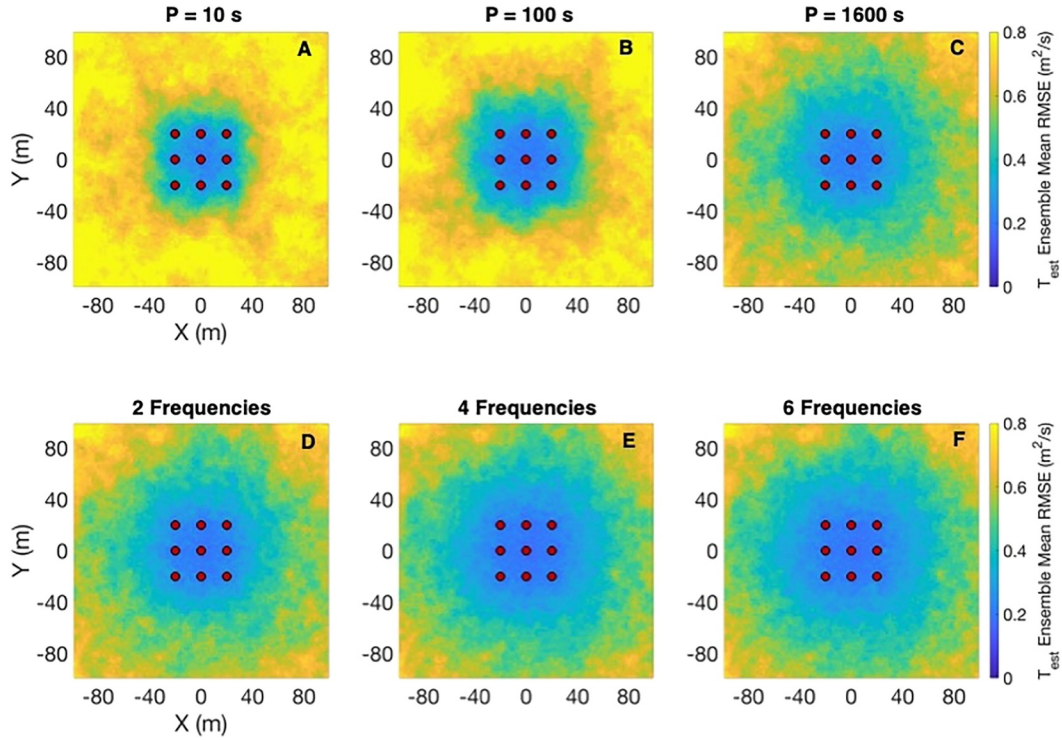

Figure 8. Transmissivity ensemble root mean squared error (RMSE). Top row shows ensemble RMSE for single-frequency Oscillatory Hydraulic Tomography (OHT) at (a) high, (b) intermediate, and (c) low frequencies. Bottom row shows ensemble RMSE for multi-frequency OHT using (d) two frequencies, (e) four frequencies, and (f) six frequencies. Red circles indicate well locations.

conduct inverse modeling (Section 2.3) to assess how well the inverted checkerboard recreates, or recovers, the input checkerboard. Areas throughout the model domain where the checkerboard is recovered with high fidelity are considered well resolved, while areas where the checkerboard pattern is not recreated are considered poorly resolved.

Conducting checkerboard testing at variable length scales provides insight into the smallest structural feature that multi-frequency OHT can reliably resolve. To explore this, we varied checker sizes from 20 m (consistent with well spacing) to 8 m, and conducted OHT with four frequencies for tomographic imaging. The recovered checkerboards indicate that structural features with length scales as small as half the length scale of the well spacing (i.e., 10 m) are well resolved throughout the well field (Figure 9); however, multi-frequency OHT does

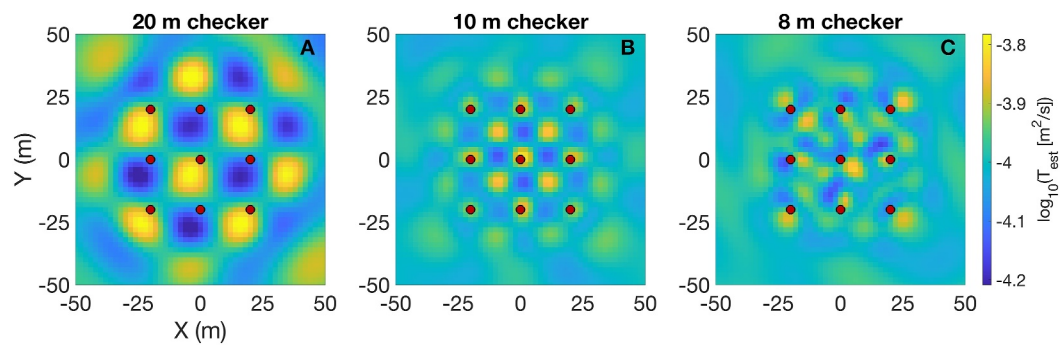

Figure 9. Inverted transmissivity checkerboards using four frequencies during inversion with (a) 20 m, (b) 10 m, and (c) 8 m checker sizes. Multi-frequency Oscillatory Hydraulic Tomography reproduces the checkerboard pattern down to a checker size of 10 m. Red circles represent well locations.

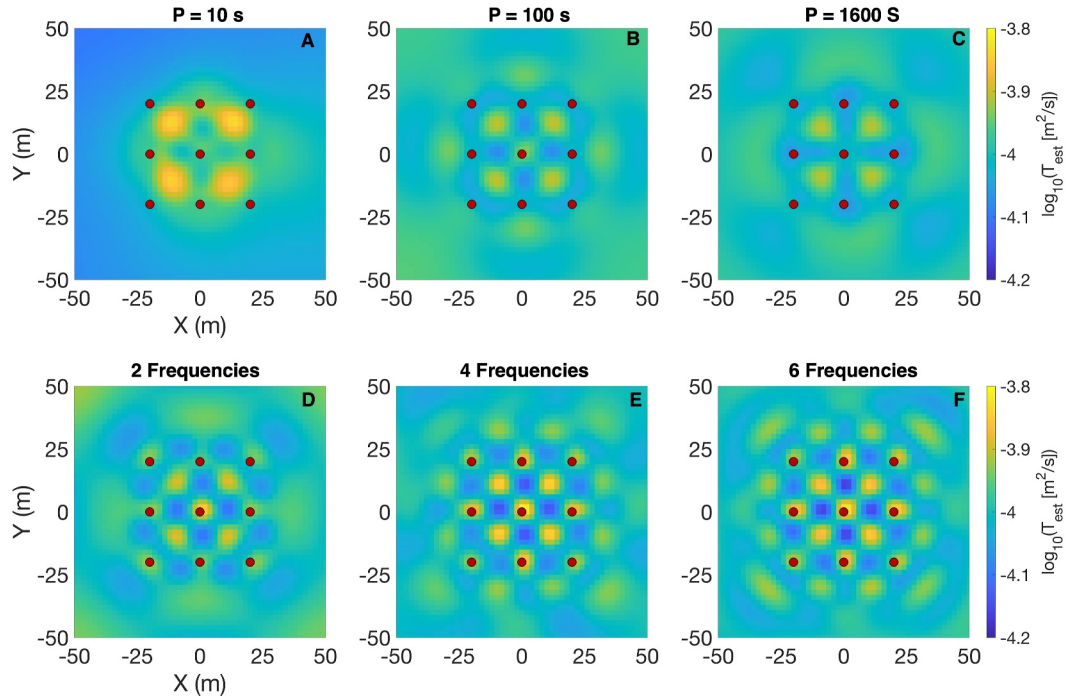

Figure 10. Inverted transmissivity checkerboards. Top row shows recovered checkerboards for single-frequency Oscillatory Hydraulic Tomography (OHT) at (a) high, (b) intermediate, and (c) low frequencies. Bottom row shows recovered checkerboards for multi-frequency OHT using (d) two frequencies, (e) four frequencies, and (f) six frequencies. Red circles represent well locations.

not resolve the structural features of the smallest checker pattern (i.e., 8 m) (Figure 9). Notably, multi-frequency OHT demonstrated the ability to resolve heterogeneity beyond the observation wells (Figure 9, right), which is a documented limitation with other HT approaches (Bohling, 2009; Paradis et al., 2015). The typical motivation of tomographic imaging is to resolve aquifer heterogeneity at the smallest possible spatial scale that accurately reproduces measured field observations; therefore, the remainder of the checkerboard analyses presented in this section utilizes the smallest resolvable length scale (i.e., 10 m checker size).

Conducting single-frequency OHT across a range of pumping frequencies reveals how the temporal scale of hydraulic stresses impacts parameter resolution—and thus information content of different frequencies. Recovered checkerboards with single-frequency OHT show that the resolution of transmissivity is dependent on the signal of the pumping frequency and is limited to the region inside the well field (Figure 10). High-frequency (10 s period) pumping signals resolve only the high transmissivity zones immediately surrounding the central well, while low transmissivity zones and regions beyond the central well show are poorly resolved. Low-frequency (1,600 s period) pumping signals generate smoothed checkerboard images with limited resolution throughout the well field, and intermediate pumping frequencies ($P = 100$ s) balance the trade-off between sharp near-field resolution and overly-smoothed large scale structure resolution (Figure 10).

The frequency-dependence of parameter resolution (i.e., checkerboard recovery) with single-frequency OHT suggests that each frequency contains unique information that could be leveraged to improve parameter resolution through tomographic imaging with multi-frequency OHT. When using two frequencies, checkerboard recovery shows that transmissivity resolution is constrained to the well field, with areas of greatest resolution concentrated around the central well (Figure 10). The additional frequency component improves resolution of low transmissivity regions that are not resolved with single-frequency OHT (Figure 10). The use of four and six frequencies during OHT sees checkerboard recovery across the entire well field, and some recovery expanding beyond the well field, suggesting the ability of multi-frequency OHT to resolve aquifer parameters beyond the well field (Figure 10).

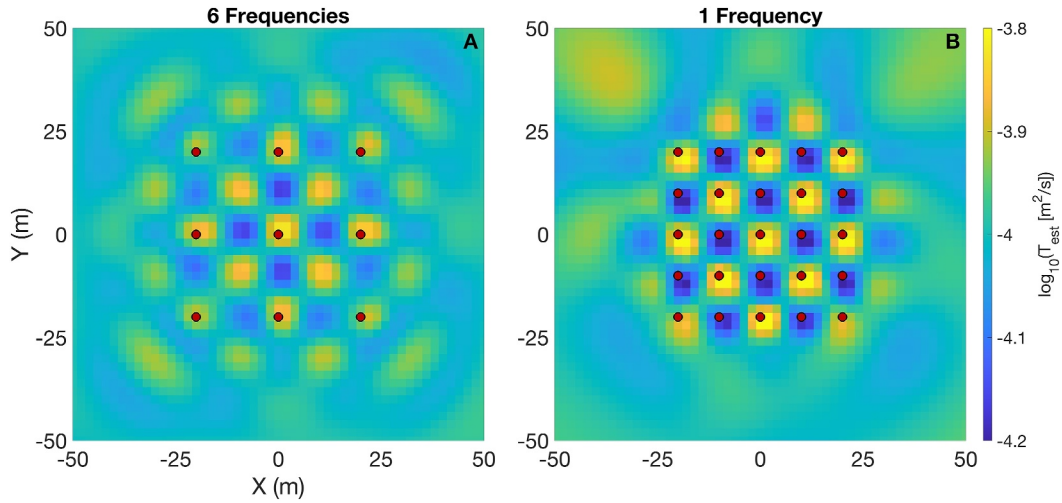

Figure 11. Inverted transmissivity checkerboards demonstrating the impact of spatial observation density on parameter resolution. (a) Multi-frequency Oscillatory Hydraulic Tomography (OHT) with 20-m well spacing closely matches the near perfect resolution of (b) single-frequency OHT with 10 m well spacing. Red circles indicate well locations.

Finally, we explore the impact of spatial observation density on model resolution, by comparing checkerboard recovery of multi-frequency OHT with 20 m well separation to single-frequency OHT checkerboard recovery with 10 m well separation. As expected, using a 10 m well separation to increase data density shows near perfect checkerboard recovery throughout the well field (Figure 11). Though the multi-frequency OHT scenario has a lower observational density, the inclusion of multi-scale hydraulic data provides information content during inverse modeling that achieves a similar level of resolution to the scenario with 10 m well separation (Figure 11). This result suggests that multi-frequency OHT provides hydraulic information content that has the potential to improve aquifer heterogeneity imaging without the increasing observation density through additional wells.

4. Discussion

The use of more data points when performing hydrogeologic imaging has always been understood to carry unique information content that improves imaging of aquifer heterogeneity. The addition of unique information during HT surveys can be through the use of additional well locations (Cardiff, Barrash, & Kitanidis, 2013; Clemo et al., 2003; Illman et al., 2015; Wen et al., 2020; Yeh & Liu, 2000; Zhao & Illman, 2018), additional temporal data points on drawdown curves (Cardiff & Barrash, 2011), and data points from hydraulic tests conducted at different temporal scales (Bohling, 2009). This may lead some practitioners and geophysicists to an intuitive conclusion that multi-frequency hydraulic data provides more information about aquifer heterogeneity relative to single-frequency hydraulic data. Indeed, the results of this study show that adding more data points, in the form of multi-frequency hydraulic data, provides unique sensitivity structures—as shown by the frequency-dependent model resolution (Figure 9)—that can be leveraged to improve inversion performance, model resolution, and parameter uncertainty.

Yet, there has been disagreement on the added value of multi-frequency hydraulic data during aquifer imaging with Wang et al. (2021) claiming that multi-frequency OHT does not improve imaging and the only way to gain more information about subsurface heterogeneity is through additional observation locations. Their claim contradicts the results of this work, which demonstrates a clear improvement in tomographic imaging and resolution when multiple frequencies are used during to characterize aquifer heterogeneity. We posit two potential reasons for this disagreement. First, the pumping frequencies chosen for our analysis span more than two orders-of-magnitude (10–1,600 s pumping period), while Wang et al. (2021) employed pumping frequencies that spans slightly less than one order-of-magnitude (15–100 s pumping period). The broad range of frequencies employed in this study takes advantage of the complementary information provided by the variable sensitivity structures across a broad range of pumping frequencies (Cardiff, Bakhos, et al., 2013), which is not available to multi-frequency hydraulic data with a narrow range of pumping frequencies that likely contain very similar sensitivity structures. Second, in another scenario Wang et al. (2021) choose exceedingly large pumping periods (400–

10,800 s pumping period) for the chosen aquifer geometry. The impact of this is that the introduced pressure signals propagate beyond the well field (their described area of interest) at all tested frequencies, thereby ignoring the frequency-dependence of the sensitivity structures and preferentially sampling the large-scale structures of the aquifer, neglecting smaller-scale heterogeneity within the well field. This discrepancy in analysis results highlights the need to carefully consider the range of frequencies implemented during OHT so that they provide the most complete information with sensitivity to both the near-field and far-field aquifer heterogeneity.

While this work demonstrates that multi-frequency OHT data improves imaging and resolution of aquifer heterogeneity, it also suggests that the frequencies employed must be chosen with care. In OHT, the frequency of the pumping signal controls the volume of aquifer—and thus the scale of heterogeneity—sampled, leading to the frequency-dependent variations in imaging, resolution, and uncertainty presented in this analysis. The implication of this frequency-dependence is that multi-frequency OHT is only beneficial when pumping frequencies are specified such that they adequately sample the aquifer at distinctly different scales. As an illustrative example, if multiple high-frequency pumping signals are chosen, the data will be biased to provide redundant information about near borehole heterogeneity, yielding minimal to no improvement in imaging, and resolution. The same holds true for multi-frequency OHT using all low-frequency data, with the exception that the tomographic imaging would be biased toward large-scale heterogeneity structures throughout the aquifer. While multi-frequency OHT improves aquifer imaging and resolution, there is a point at which the hydraulic data provided by adding another frequency yields diminishing returns on imaging due to the addition of primarily redundant information content. The number of frequencies at which this occurs will be site specific and is likely controlled by the degree of heterogeneity present within the aquifer. Highly heterogeneous aquifers containing large contrasts in aquifer parameters will require greater frequency content to fully sample the heterogeneity at all scales present within the aquifer, whereas more uniform aquifer systems can be adequately characterized with fewer frequency components.

The hydraulic and geostatistical parameters chosen for this work are representative of an alluvial aquifer system with transmissivity heterogeneity that spans approximately three orders-of-magnitude, with generally smooth transitions from high-transmissivity to low-transmissivity regions throughout the aquifer. In deeper bedrock aquifer settings, subsurface flow and transports tends to be concentrated along high-transmissivity conduits such as fractures and faults. The small size of these features relative to the aquifer system and the sharp contrast in hydraulic parameters, which can vary by multiple orders-of-magnitude over small spatial scales presents an additional challenge when imaging aquifer heterogeneity. Traditional HT approaches have been shown to capture the juxtaposition of high- and low-transmissivity regions in highly heterogeneous aquifers (Hochstetler et al., 2016) and bedrock aquifers where flow is dominated by individual fractures or connected fracture networks (Illman, 2014; Tiedeman & Barrash, 2020). Given the success of traditional tomographic approaches to image these highly heterogeneous aquifers, the ability of multi-frequency OHT to add hydraulic data across a range of scales suggests that the results of this work would be generalizable to these settings and improve tomographic imaging relative to traditional HT, similar to Cardiff et al. (2020). However, multi-frequency OHT in aquifers with juxtaposed high- and low-transmissivity zones remains largely unexplored, with only one study that we're aware of attempting to image karst conduit geometries (Fischer et al., 2018). We should note, that tomographic imaging studies in fractured bedrock should be approached with skepticism as underlying assumptions (e.g., fracture rigidity) are likely violated (Patterson & Cardiff, 2023b), which would have a direct impact on the resulting tomograms, especially if the storage coefficient is treated as a heterogeneous invertible parameter.

The resolution and uncertainty results presented in this analysis are, of course, directly tied to the chosen model configuration and testing parameters. As an initial investigation into the resolution associated with OHT, the modeling decisions made in this work represent highly idealized conditions that lead to resolution likely being artificially inflated and uncertainty being underestimated compared to more realistic field scenarios. For example, allowing 3D head propagation throughout the aquifer would result in a decrease in parameter resolution and an increase in the length scale of structures that could be reliably resolved. Similarly, reducing the number of pumping locations used during OHT similar to Wang et al. (2021) would also lead to a decrease in resolution, resulting from a decrease in flow path density, and thus heterogeneity sampling, throughout the aquifer. Similarly, reducing the number of wells or changing the geometry of the well field will decrease flow path densities throughout the area of interest, leading to a decrease in parameter resolution within the well field. Despite these limitations, the trends of improved heterogeneity imaging and resolution when using multiple frequencies during tomographic analysis are generalizable insights that can be applied to these non-ideal settings, when the pumping

frequencies are selectively chosen to ensure they all sample different scales of the aquifer and thus have differing sensitivity structures.

Due to the specialized equipment required for data collection and the computational demand required for numerical modeling analysis, tomographic approaches to aquifer characterization have been criticized for requiring a level of expense, expertise, and field effort that presents a potential barrier for adoption by the practicing hydrogeologist (Bohling & Butler Jr, 2010). As a tomographic imaging method, OHT is subject to similar and additional criticisms, specifically the time required to implement multi-frequency OHT in a field setting. A single oscillatory flow test will always take longer to conduct compared to a constant-rate pumping test of the same temporal scaling. This could add to the total work hours required to complete an OHT survey if multiple frequencies are employed. However, because repeat oscillatory flow tests can be run with no downtime waiting for aquifer recovery, it is possible that a single-frequency OHT campaign could be conducted in a similar time as a THT campaign of similar temporal scaling depending on the amount of quiescent time required for aquifer recovery between each constant-rate pumping test. Though multi-frequency OHT generally requires more labor hours, the improved resolution reduces the need for additional wells during characterization efforts, which could ultimately result in reduced overall testing costs, dependent on well installation requirements. Further, recent field experiments that have demonstrated improvements in the detail of heterogeneity imaging (Cardiff et al., 2020), suggest a return on the investment of additional labor costs by allowing for more accurate optimization of site operations. A strategy to reduce the time required for multi-frequency OHT would be to introduce a multi-frequency pumping signal into the aquifer as opposed to conducting multiple single-frequency oscillatory flow tests, which is a strategy that remains unexplored to date.

An open question that continues to elude groundwater practitioners is what hydraulic testing methods, if any, are capable of characterizing variability in aquifer properties at the kilometer scale (1–10 km^2). The frequencies used in this study are appropriate for characterizing heterogeneity from scales from tens to hundreds of meters, and are indicative of the range of frequencies that can be expected to be imposed under realistic field testing conditions (Cardiff et al., 2020; Guiltinan & Becker, 2015; Patterson & Cardiff, 2023a; Sayler et al., 2018). The development of equipment designed to manually introduce oscillations at frequencies and amplitudes sufficient to sample these larger scales is likely a difficult proposition. However, there are a number of natural processes—river stage fluctuations, evapotransporation, tides (ocean and solid Earth), etc…—that have been shown to generate hydraulic signals of sufficient amplitude and frequency to characterize effective (or homogeneous) aquifer properties (e.g., Allègre et al., 2016; McMillan et al., 2019; Rau et al., 2022; Valois et al., 2022), and therefore these signals should be useful for identifying aquifer heterogeneity at these larger scales. These natural processes that generate oscillatory signals occurring on daily or longer timescales represents a largely untapped source of passive data for large-scale aquifer heterogeneity characterization.

5. Conclusions

Accurate and effective characterization of multi-scale aquifer heterogeneity remains a critical research priority in the face of increasingly stressed and diminishing groundwater supplies. OHT represents a minimally invasive aquifer characterization technique that is seeing increased use in field applications and showing promise for multi-scale imaging of aquifer heterogeneity by tuning the frequency of the pumping signal. OHT data benefits from a well-developed suite of signal processing tools that can simplify analysis by extracting small amplitude signals of a known frequency from noisy data, making it ideal for application in field settings. Whereas, traditional HT that relies on constant-rate pumping tests present additional analysis and modeling challenges as these signals can record multiple forms of hydrologic noise that are not easily deconvolved and add complexity to modeling efforts, introduced oscillatory signals can be easily extracted from these spurious forms of hydrologic and/or instrument noise and easily modeled using the approaches described throughout this work. The ability to easily extract these small amplitude signals from noisy data creates significant implications for long-term aquifer monitoring and permeability evolution.

The increased use of oscillatory signals for aquifer characterization has led to a lack of consensus as to whether the use of multiple frequencies during OHT improves imaging of aquifer heterogeneity. This work represents one of the first studies that applied a range of commonly applied geophysical analysis techniques to explore the imaging, resolution, and uncertainty associated with OHT in a systematic way. Consistent with what seismologists have known for some time in the context of analyzing subsurface vibrations, we demonstrated that the use of multiple

frequencies during hydraulic testing leads to data that improves tomographic imaging and resolution, while decreasing parameter uncertainties. Though multi-frequency OHT improves imaging, the chosen frequencies be should chosen with care to ensure that each frequency generates data that maximizes unique information content and minimizes redundancy. The multi-scale, high-resolution imaging capability makes multi-frequency OHT an attractive aquifer characterization approach with potential to overcome the limitations of more traditional hydraulic characterization approaches.

Nomenclature

b	Aquifer thickness (m)
f	Oscillation frequency (1/s)
g	Acceleration due to gravity (m/s^2)
h	Hydraulic head (m)
h'	Oscillatory head change (m)
i	Imaginary number $\sqrt{-1}$
$\mathbf{J}$	Jacobian (sensitivity) matrix
L_x	X correlation length (m)
L_y	Y correlation length (m)
m	Number of parameters
n	Number of data
P	Oscillation period (s)
$\mathbf{Q_s}$	Parameter covariance matrix
$\mathbf{Q_y}$	Data error covariance matrix
q	Pumping signal (m^3/s)
S	Storativity (−)
S_s	Specific storage (1/m)
T	Transmissivity (m^2/s)
t	Time (s)
$\mathbf{x}$	Spatial coordinate vector (m)
β_f	Fluid compressibility (1/Pa)
β_r	Rock compressibility (1/Pa)
η	Porosity (−)
Γ_d	Specified head (Dirichlet) boundary condition (m)
Γ_n	Specified flux (Neumann) boundary condition (m/s)
κ	Permeability (m^2)
μ_f	Fluid viscosity (Pa·s)
Ω	Model Domain
ω	Angular frequency (rad/s)
ρ	Pearson correlation coefficient (−)
ρ_f	Fluid density (kg/m^3)

Acknowledgments
This work was supported by funding from the National Science Foundation Grants NSF-EAR 1654649 "CAREER: Understanding Transport Processes in Fractured Sedimentary Rock Through Multi-Frequency and Multi-Method Investigations" and NSF-EAR 2204543 "EAR-PF: Dynamic flow channeling through complex fracture networks under multi-frequency oscillatory flow conditions: A fully-coupled hydromechanical approach." We are grateful to the associate editor, Dr. Lisa Ringel, and 2 anonymous reviewers, whose comments greatly improved the quality of this work.

Data Availability Statement

No new data was presented in this manuscript. All code used to recreate the analysis presented in this work can be found at Zenodo (Patterson & Cardiff, 2024). The inverse modeling software OHT3DINV v0.16.0 is available on Github (Cardiff, 2016).

References

Allègre, V., Brodsky, E. E., Xue, L., Nale, S. M., Parker, B. L., & Cherry, J. A. (2016). Using earth-tide induced water pressure changes to measure in situ permeability: A comparison with long-term pumping tests. *Water Resources Research*, *52*(4), 3113–3126. https://doi.org/10.1002/2015WR017346

Aster, R. C., Borchers, B., & Thurber, C. H. (2018). *Parameter estimation and inverse problems* (3rd ed.). Elsevier.

Bakhos, T., Cardiff, M., Barrash, W., & Kitanidis, P. K. (2014). Data processing for oscillatory pumping tests. *Journal of Hydrology*, *511*, 310–319. https://doi.org/10.1016/j.jhydrol.2014.01.007

Binley, A., Hubbard, S. S., Huisman, J. A., Revil, A., Robinson, D. A., Singha, K., & Slater, L. D. (2015). The emergence of hydrogeophysics for improved understanding of subsurface processes over multiple scales. *Water Resources Research*, *51*(6), 3837–3866. https://doi.org/10.1002/2015WR017016

Bohling, G. C. (2009). Sensitivity and resolution of tomographic pumping tests in an alluvial aquifer. *Water Resources Research*, *45*(2), W02420. https://doi.org/10.1029/2008WR007249

Bohling, G. C., & Butler Jr, J. J. (2010). Inherent limitations of hydraulic tomography. *Groundwater Series*, *48*(6), 809–824. https://doi.org/10.1111/j.1745-6584.2010.00757.x

Bohling, G. C., Butler Jr, J. J., Zhan, X., & Knoll, M. D. (2007). A field assessment of the value of steady shape hydraulic tomography for characterization of aquifer heterogeneities. *Water Resources Research*, *43*(5). https://doi.org/10.1029/2006wr004932

Cardiff, M. (2016). OHT3DINV [Software]. https://github.com/wischydro-cardiff/oscillatory-tomography

Cardiff, M., Bakhos, T., Kitanidis, P. K., & Barrash, W. (2013). Aquifer heterogeneity characterization with oscillatory pumping: Sensitivity analysis and imaging potential. *Water Resources Research*, *49*(9), 5395–5410. https://doi.org/10.1002/wrcr.20356

Cardiff, M., & Barrash, W. (2011). 3-D transient hydraulic tomography in unconfined aquifers with fast drainage response. *Water Resources Research*, *47*(12), W12518. https://doi.org/10.1029/2010WR010367

Cardiff, M., Barrash, W., & Kitanidis, P. K. (2013). Hydraulic conductivity imaging from 3-D transient hydraulic tomography at several pumping/observation densities. *Water Resources Research*, *49*(11), 7311–7326. https://doi.org/10.1002/wrcr.20519

Cardiff, M., Barrash, W., Kitanidis, P. K., Malama, B., Revil, A., Straface, S., & Rizzo, E. (2009). A potential-based inversion of unconfined steady-state hydraulic tomography. *Groundwater Series*, *47*(2), 259–270. https://doi.org/10.1111/j.1745-6584.2008.00541.x

Cardiff, M., Zhou, Y., Barrash, W., & Kitanidis, P. K. (2020). Aquifer imaging with oscillatory hydraulic tomography: Application at the field scale. *Groundwater Series*, *58*(5), 710–722. https://doi.org/10.1111/gwat.12960

Clemo, T., Michaels, P., & Lehman, R. M. (2003). Transmissivity resolution obtained from the inversion of transient and pseudo-steady drawdown measurements. In *Proceedings of MODFLOW and more 2003: Understanding through modeling* (pp. 629–633). Integrated Groundwater Modeling Center.

Cuss, R. J., Harrington, J. F., Noy, D. J., Sathar, S., & Norris, S. (2015). An experimental study of the flow of gas along synthetic faults of varying orientation to the stress field: Implications for performance assessment of radioactive waste disposal. *Journal of Geophysical Research: Solid Earth*, *120*(5), 3932–3945. https://doi.org/10.1002/2014JB011333

Day-Lewis, F. D., Slater, L. D., Robinson, J., Johnson, C. D., Terry, N., & Werkema, D. (2017). An overview of geophysical technologies appropriate for characterization and monitoring at fractured-rock sites. *Global Trends in the Environmental Remediation Industry*, *204*, 709–720. https://doi.org/10.1016/j.jenvman.2017.04.033

Domenico, P. A., & Schwartz, F. W. (1997). *Physical and chemical hydrogeology* (2nd ed.). John Wiley and Sons.

Fischer, P., Jardani, A., Jourde, H., Cardiff, M., Wang, X., Chedeville, S., & Lecoq, N. (2018). Harmonic pumping tomography applied to image the hydraulic properties and interpret the connectivity of a karstic and fractured aquifer (Lez aquifer, France). *Advances in Water Resources*, *119*, 227–244. https://doi.org/10.1016/j.advwatres.2018.07.002

Freeze, R. A., & Cherry, J. A. (1979). *Groundwater* (1st ed.). Prentice-Hall.

Fu, P., Settgast, R. R., Hao, Y., Morris, J. P., & Ryerson, F. J. (2017). The influence of hydraulic fracturing on carbon storage performance. *Journal of Geophysical Research: Solid Earth*, *122*(12), 9931–9949. https://doi.org/10.1002/2017JB014942

Guiltinan, E., & Becker, M. W. (2015). Measuring well hydraulic connectivity in fractured bedrock using periodic slug tests. *Journal of Hydrology*, *521*, 100–107. https://doi.org/10.1016/j.jhydrol.2014.11.066

Hearn, T. M., & Ni, J. F. (1994). Pn velocities beneath continental collision zones: The Turkish-Iranian Plateau. *Geophysical Journal International*, *117*(2), 273–283. https://doi.org/10.1111/j.1365-246X.1994.tb03931.x

Hochstetler, D. L., Barrash, W., Leven, C., Cardiff, M., Chidichimo, F., & Kitanidis, P. K. (2016). Hydraulic tomography: Continuity and discontinuity of high-K and low-K zones. *Groundwater Series*, *54*(2), 171–185. https://doi.org/10.1111/gwat.12344

Hou, X., Hu, R., Yeh, T.-C. J., Li, Y., Qi, J., Song, Y., & Qiu, H. (2023). A short-term pumping strategy for hydraulic tomography based on the successive linear estimator. *Water Resources Research*, *59*(4), e2022WR033831. https://doi.org/10.1029/2022WR033831

Illman, W. A. (2014). Hydraulic tomography offers improved imaging of heterogeneity in fractured rocks. *Groundwater Series*, *52*(5), 659–684. https://doi.org/10.1111/gwat.12119

Illman, W. A., Berg, S. J., & Zhao, Z. (2015). Should hydraulic tomography data be interpreted using geostatistical inverse modeling? A laboratory sandbox investigation. *Water Resources Research*, *51*(5), 3219–3237. https://doi.org/10.1002/2014WR016552

Illman, W. A., Liu, X., Takeuchi, S., Yeh, T.-C. J., Ando, K., & Saegusa, H. (2009). Hydraulic tomography in fractured granite: Mizunami Underground Research site, Japan. *Water Resources Research*, *45*(1), W01406. https://doi.org/10.1029/2007WR006715

Kitanidis, P. K. (1995). Quasi-linear geostatistical theory for inversing. *Water Resources Research*, *31*(10), 2411–2419. https://doi.org/10.1029/95WR01945

Leven, C., & Barrash, W. (2022). Fiber optic pressure measurements open up new experimental possibilities in hydrogeology. *Groundwater Series*, *60*(1), 125–136. https://doi.org/10.1111/gwat.13128

McClure, M. W., & Horne, R. N. (2014). An investigation of stimulation mechanisms in Enhanced Geothermal Systems. *International Journal of Rock Mechanics and Mining Sciences*, *72*, 242–260. https://doi.org/10.1016/j.ijrmms.2014.07.011

McMillan, T. C., Rau, G. C., Timms, W. A., & Andersen, M. S. (2019). Utilizing the impact of earth and atmospheric tides on groundwater systems: A review reveals the future potential. *Reviews of Geophysics*, *57*(2), 281–315. https://doi.org/10.1029/2018RG000630

Paradis, D., Gloaguen, E., Lefebvre, R., & Giroux, B. (2015). Resolution analysis of tomographic slug test head data: Two-dimensional radial case. *Water Resources Research*, *51*(4), 2356–2376. https://doi.org/10.1002/2013WR014785

Paradis, D., Lefebvre, R., & Nefzi, A. (2024). Parameter resolution of simulated responses to periodic hydraulic tomography signals in aquifers. *Advances in Water Resources*, *190*, 104734. https://doi.org/10.1016/j.advwatres.2024.104734

Patterson, J. R., & Cardiff, M. (2022a). Aquifer characterization and uncertainty in multi-frequency oscillatory flow tests: Approach and insights. *Groundwater Series*, *60*(2), 180–191. https://doi.org/10.1111/gwat.13134

Patterson, J. R., & Cardiff, M. (2022b). Spectral hydrology: Resolution and uncertainty in multifrequency oscillatory hydraulic tomography. In *Second international meeting for applied geoscience and energy* (pp. 3128–3132). Society of Exploration Geophysicists and American Association of Petroleum Geologists. https://doi.org/10.1190/image2022-3745974.1

Patterson, J. R., & Cardiff, M. (2023a). Do simple analytical models capture complex fractured bedrock hydraulics? Oscillatory flow tests suggest not. *Groundwater Series*, *61*(6), 816–833. https://doi.org/10.1111/gwat.13297

Patterson, J. R., & Cardiff, M. (2023b). Stiff, smooth, and solid? Complex fracture hydraulics' imprint on oscillatory hydraulic testing. *Water Resources Research*, *59*(11), e2023WR034621. https://doi.org/10.1029/2023WR034621

Patterson, J. R., & Cardiff, M. (2024). OHT-resolution code [Computational Notebook]. https://doi.org/10.5281/zenodo.14262598

Rasmussen, T. C., Haborak, K. G., & Young, M. H. (2003). Estimating aquifer hydraulic properties using sinusoidal pumping at the Savannah River site, South Carolina, USA. *Hydrogeology Journal*, *11*(4), 466–482. https://doi.org/10.1007/s10040-003-0255-7

Rau, G. C., Acworth, R. I., Halloran, L. J. S., Timms, W. A., & Cuthbert, M. O. (2018). Quantifying compressible groundwater storage by combining cross-hole seismic surveys and head response to atmospheric tides. *Journal of Geophysical Research: Earth Surface*, *123*(8), 1910–1930. https://doi.org/10.1029/2018JF004660

Rau, G. C., McMillan, T. C., Andersen, M. S., & Timms, W. A. (2022). In situ estimation of subsurface hydro-geomechanical properties using the groundwater response to semi-diurnal Earth and atmospheric tides. *Hydrology and Earth System Sciences*, *26*(16), 4301–4321. https://doi.org/10.5194/hess-26-4301-2022

Rawlinson, N., & Spakman, W. (2016). On the use of sensitivity tests in seismic tomography. *Geophysical Journal International*, *205*(2), 1221–1243. https://doi.org/10.1093/gji/ggw084

Sanchez-Vila, X., Guadagnini, A., & Carrera, J. (2006). Representative hydraulic conductivities in saturated groundwater flow. *Reviews of Geophysics*, *44*(3), RG3002. https://doi.org/10.1029/2005RG000169

Sayler, C., Cardiff, M., & Fort, M. D. (2018). Understanding the geometry of connected fracture flow with multiperiod oscillatory hydraulic tests. *Groundwater Series*, *56*(2), 276–287. https://doi.org/10.1111/gwat.12580

Singha, K. (2017). Geophysics is not a silver bullet, but worth a shot. *Groundwater Series*, *55*(2), 149. https://doi.org/10.1111/gwat.12495

Sun, R., Yeh, T.-C. J., Mao, D., Jin, M., Lu, W., & Hao, Y. (2013). A temporal sampling strategy for hydraulic tomography analysis. *Water Resources Research*, *49*(7), 3881–3896. https://doi.org/10.1002/wrcr.20337

Sun, Y., & Tong, C. (2017). Dynamic reduced-order models of integrated physics-specific systems for carbon sequestration. *Geomechanics and Geophysics for Geo-Energy and Geo-Resources*, *3*(3), 315–325. https://doi.org/10.1007/s40948-017-0061-7

Tiedeman, C. R., & Barrash, W. (2020). Hydraulic tomography: 3D hydraulic conductivity, fracture network, and connectivity in mudstone. *Groundwater Series*, *58*(2), 238–257. https://doi.org/10.1111/gwat.12915

Tsang, C.-F., Neretnieks, I., & Tsang, Y. (2015). Hydrologic issues associated with nuclear waste repositories. *Water Resources Research*, *51*(9), 6923–6972. https://doi.org/10.1002/2015WR017641

Valois, R., Rau, G. C., Vouillamoz, J.-M., & Derode, B. (2022). Estimating hydraulic properties of the shallow subsurface using the groundwater response to earth and atmospheric tides: A comparison with pumping tests. *Water Resources Research*, *58*(5), e2021WR031666. https://doi.org/10.1029/2021WR031666

Vasco, D. W., Datta-Gupta, A., & Long, J. C. (1997). Resolution and uncertainty in hydrologic characterization. *Water Resources Research*, *33*(3), 379–397. https://doi.org/10.1029/96WR03301

Wang, Y.-L., Yeh, T.-C. J., Xu, D., Li, K., Wen, J.-C., Huang, S.-Y., et al. (2021). Stochastic analysis of oscillatory hydraulic tomography. *Journal of Hydrology*, *596*, 126105. https://doi.org/10.1016/j.jhydrol.2021.126105

Wen, J.-C., Chen, J.-L., Yeh, T.-C. J., Wang, Y.-L., Huang, S.-Y., Tian, Z., & Yu, C.-Y. (2020). Redundant and nonredundant information for model calibration or hydraulic tomography. *Groundwater Series*, *58*(1), 79–92. https://doi.org/10.1111/gwat.12879

Wu, H., Fu, P., Morris, J. P., Mattson, E. D., Neupane, G., Smith, M. M., et al. (2021). Characterization of flow and transport in a fracture network at the EGS Collab field experiment through stochastic modeling of tracer recovery. *Journal of Hydrology*, *593*, 125888. https://doi.org/10.1016/j.jhydrol.2020.125888

Yeh, T.-C. J., & Liu, S. (2000). Hydraulic tomography: Development of a new aquifer test method. *Water Resources Research*, *36*(8), 2095–2105. https://doi.org/10.1029/2000WR900114

Zelt, C. A. (1998). Lateral velocity resolution from three-dimensional seismic refraction data. *Geophysical Journal International*, *135*(3), 1101–1112. https://doi.org/10.1046/j.1365-246X.1998.00695.x

Zhao, Z., & Illman, W. A. (2018). Three-dimensional imaging of aquifer and Aquitard heterogeneity via transient hydraulic tomography at a highly heterogeneous field site. *Journal of Hydrology*, *559*, 392–410. https://doi.org/10.1016/j.jhydrol.2018.02.024

Zhou, Y., & Cardiff, M. (2017). Oscillatory hydraulic testing as a strategy for NAPL source zone monitoring: Laboratory experiments. *Journal of Contaminant Hydrology*, *200*, 24–34. https://doi.org/10.1016/j.jconhyd.2017.03.005

Zhou, Y., Lim, D., Cupola, F., & Cardiff, M. (2016). Aquifer imaging with pressure waves—Evaluation of low-impact characterization through sandbox experiments. *Water Resources Research*, *52*(3), 2141–2156. https://doi.org/10.1002/2015WR017751